

Dynamics of entanglement in the one-dimensional anisotropic XXZ model

Han Zhang^a, Yu-Liang Xu^b, Rong-Tao Zhang^a, Zhe Wang^a,
Pan-Pan Fang^a, Zhong-Qiang Liu^a, and Xiang-Mu Kong^{a,b*}

^a*College of Physics and Engineering,*

Qufu Normal University, Qufu 273165, China

^b*School of Physics and Optoelectronic Engineering,*

Ludong University, Yantai 264025, China

Abstract

The dynamics of entanglement in the one-dimensional spin-1/2 anisotropic XXZ model is studied using the quantum renormalization-group method. We obtain the analytical expression of the concurrence, for two different quenching methods, it is found that initial state plays a key role in the evolution of system entanglement, i.e., the system returns completely to the initial state every other period ($T = \frac{4\pi}{\sqrt{8+\gamma^2}}$). Our computations and analysis indicate that the first derivative of the characteristic time at which the concurrence reaches its maximum or minimum with respect to the anisotropic parameter occurs nonanalytic behaviors at the quantum critical point. Interestingly, the minimum value of the first derivative of the characteristic time versus the size of the system exhibits the scaling behavior which is the same as the scaling behavior of the system ground-state entanglement in equilibrium. In particular, the scaling behavior near the critical point is independent of the initial state.

PACS numbers: 03.67.Mn; 64.60.ae; 64.70.Tg; 75.10.Jm.

Keywords: Entanglement dynamics; Quantum renormalization group; Quantum XXZ model; Time-dependent density matrix.

*Corresponding author.

E-mail address: kongxm668@163.com(X.-M. Kong).

1. INTRODUCTION

A fundamental difference between quantum and classical physics is that there is nonclassical correlation in quantum systems called quantum entanglement [1] which not counterpart in classical systems. Therefore, the quantum entanglement is considered as an important resource in quantum information and quantum computation [1, 2]. In addition, quantum entanglement also plays a significant role in the quantum phase transition (QPT). Due to the correlation length diverges at the quantum critical points, the entanglement is a good index of QPTs [3–5]. In the past few years, the behavior of entanglement at the vicinity of quantum critical point has been studied in various spin models [6–13], which has achieved great success in theoretically.

Recent advances in experimental technologies, for instance the cold atoms, trapped ions [14] and ultrafast pulsed lasers [15], have made it possible to study the dynamics of nonequilibrium quantum many-body systems. In addition, not only studies the entanglement dynamics in many-body spin systems help us understanding the essence of dynamical quantum phase transition, but it also provides a possible theoretical reference for the design of solid-state quantum computer. Therefore, the entanglement dynamics of many-body quantum systems has attracted widespread attention in recent years. The entanglement dynamics have been studied in recent years mainly from the following two different perspectives. On the one hand, some work studied the propagation of entanglement start from a initial state that the entanglement has been created in a given portion of the multi-body system [16–18]. On the other hand, the Hamiltonian changed in time from a certain ground state of a Hamiltonian H_0 . Recent advances have demonstrated the effectiveness of a quantum quenching approach for the study of the entanglement dynamics in many-body spin systems [19–23]. For example, the adaptive time-dependent density-matrix renormalization group was applied to discuss the quantum entanglement dynamics of an open anisotropic spin- $\frac{1}{2}$ Heisenberg chain [19]. The properties of entanglement dynamics in the ITM were also studied by the quantum renormalization group [20]. However, the ground state fidelity and quench dynamics of the 1D extended quantum compass model in a transverse field were investigated [22], which indicate that the fidelity susceptibility and LE could detect the QPTs in the inhomogeneous system. In particular, the dynamical quantum phase transitions of an interacting many-body system has been observed experimentally [21]. Previous research

dedicated to understanding the general properties of nonequilibrium quantum states and expanding significant concepts such as universality to nonequilibrium regime. In this paper, we show that the low-energy-state dynamical quantities of one-dimensional XXZ model can detect the QPTs of the system, which is universal.

In equilibrium, the entanglement and quantum phase transition of a spin- $\frac{1}{2}$ anisotropic Heisenberg chain has been discussed in Ref. [7]. In this paper, the entanglement dynamics of one-dimensional XXZ model is studied using the quantum renormalization group method. It is found that the entanglement presents cosine variations with time for anisotropic interaction quench, whereas entanglement is sine variable with time for spin direction quench. Yet, these two different quench methods correspond to the same period, which are discussed in detail in the Sec. 3. In addition, the evolution behavior of entanglement with respect to anisotropy parameter, for two quenching methods, is dramatical different, but both of them appear singular behavior at the quantum critical point. To gain further insight, the nonanalytic behavior and scaling behavior of the entanglement dynamics are studied.

The organization of this paper is as follows. In Sec. 2 we introduce the idea of quantum renormalization group and apply it to the one-dimensional XXZ model. In Sec. 3 the entanglement dynamics of spin chain are studied when perform two kinds of typical quench. We summarize in Sec. 4.

2. QUANTUM RENORMALIZATION GROUP

We introduce the QRG method whose main idea is the elimination or thinning of the degrees of freedom of the system followed by an iteration. The purpose of iteration is to gradually reduce the number of variables until a fixed point is reached. In this paper, the Kadanoff's block approach is applied to the XXZ model, where the lattice is divided into three sites as a block. Each block can construct the projection operator onto their lower eigenvectors. The full Hamiltonian is projected onto these eigenvectors to obtain the effective Hamiltonian which has structural similarities to the original Hamiltonian [23, 24]. The specific operation is as follows, the Hamiltonian of the XXZ model on a periodic chain with N sites can be written as

$$H(J, \Gamma) = \frac{1}{4} \sum_i^N [J (\sigma_i^x \sigma_{i+1}^x + \sigma_i^y \sigma_{i+1}^y) + \Gamma \sigma_i^z \sigma_{i+1}^z], \quad (1)$$

where J is the exchange coupling constant, $J > 0$ corresponds to the antiferromagnetic system and $J < 0$ corresponds to the ferromagnetic system, here we only study the situation of antiferromagnetic system. $\gamma = \frac{\Gamma}{J}$ is the anisotropy parameter, and σ_i^α ($\alpha = x, y, z$) are Pauli matrices of the i th site.

Eq. (1) can be written as $H = H^B + H^{BB}$ by applying the Kadanoff's block approach. Here $H^B = \sum_{I=1}^{\frac{N}{3}} h_I^B$, with $h_I^B = \frac{1}{4}[J(\sigma_{I,1}^x \sigma_{I,2}^x + \sigma_{I,2}^x \sigma_{I,3}^x + \sigma_{I,1}^y \sigma_{I,2}^y + \sigma_{I,2}^y \sigma_{I,3}^y) + \Gamma(\sigma_{I,1}^z \sigma_{I,2}^z + \sigma_{I,2}^z \sigma_{I,3}^z)]$, is the block Hamiltonian. The $H^{BB} = \frac{1}{4} \sum_{I=1}^{\frac{N}{3}} [J(\sigma_{I,3}^x \sigma_{I+1,1}^x + \sigma_{I,3}^y \sigma_{I+1,1}^y) + \Gamma \sigma_{I,3}^z \sigma_{I+1,1}^z]$ is the interblock Hamiltonian. In terms of matrix product space, the Hamiltonian of each block (h_I^B) can be exactly diagonalized and get two degenerate ground states which are used to construct the projection operator ($T = |\varphi_0\rangle\langle\uparrow| + |\varphi'_0\rangle\langle\downarrow|$). Where $|\varphi_0\rangle$ and $|\varphi'_0\rangle$ are the two degenerate ground states of the block Hamiltonian (h_I^B), $|\uparrow\rangle$ and $|\downarrow\rangle$ are the renormalization change effective basis vector of the each block spin operator. Therefore, the effective Hamiltonian [$H^{eff} = T^+(H^B + H^{BB})T$] by the original Hamiltonian and the projection operator can be written as

$$H^{eff} = \frac{1}{4} \left(\sum_I^{\frac{N}{3}} [J'(\sigma_I^x \sigma_{I+1}^x + \sigma_I^y \sigma_{I+1}^y) + \Gamma' \sigma_I^z \sigma_{I+1}^z] \right), \quad (2)$$

where

$$J' = \frac{16J^3 k^2}{(8J^2 + k^2)^2}, \quad \Gamma' = \frac{k^4 \Gamma}{(8J^2 + k^2)^2}, \quad k = \Gamma + \sqrt{8J^2 + \Gamma^2}. \quad (3)$$

Eq. (3) is the QRG equations. We define a dimensionless anisotropy parameter $\gamma = \Gamma/J$ which determines the phase transition properties of the system. The QRG equations can also be written as

$$\gamma' = \frac{\gamma}{16}(\gamma + q)^2, \quad q = \sqrt{8 + \gamma^2}. \quad (4)$$

The stable and unstable fixed points can be obtained by solving $\gamma \equiv \gamma' \equiv \gamma^*$. The stable fixed points locate at $\gamma = 0$ and $\gamma = \infty$, the unstable fixed point is $\gamma = 1$ which is the critical point of the model. As the number of QRG iterations increase, starting with any initial values for $\gamma > 1$, the coupling parameter flows toward infinity indicating that the system falls into the universality class of Ising model. But for $\gamma < 1$ the stable fixed point ($\gamma = 0$) is touched. The model expresses a spin fluid phase when $0 \leq \gamma \leq 1$, $\gamma > 1$ the model expresses a Néel phase.

3. ENTANGLEMENT DYNAMICS

In this section, the entanglement dynamics of XXZ spin chain is analyzed when the anisotropic interaction and the spin direction are quenched. The following these two kinds of quenches process will be discussed in detail.

3.1. Anisotropic interaction quench

We consider that the spin chain is initialized on one of the two degenerate ground states $|\varphi_{01}\rangle$ of the XX model. Experimentally, the initial state can be obtained by adding an otherwise inconsequential infinitesimal magnetic field to the XXZ model [25]. In terms of matrix product state [26], the ground state $|\varphi_{01}\rangle$ ($|\varphi_{01}\rangle = \frac{1}{2} |\uparrow\uparrow\downarrow\rangle - \frac{\sqrt{2}}{2} |\uparrow\downarrow\uparrow\rangle + \frac{1}{2} |\downarrow\uparrow\uparrow\rangle$) of the three-site XX model can be obtained, here $|\uparrow\rangle$ and $|\downarrow\rangle$ are eigenvector of σ^z . The anisotropic interaction parameter suddenly increases from zero when time $t = 0$. In other words, the Hamiltonian is suddenly converted from H_{01} into H , where H is the Hamiltonian of the XXZ model. The system state evolves to $|\varphi_1(t)\rangle = e^{-iHt} |\varphi_{01}\rangle$, here

$$|\varphi_1(t)\rangle = a1 |\uparrow\uparrow\downarrow\rangle + b1 |\uparrow\downarrow\uparrow\rangle + a1 |\downarrow\uparrow\uparrow\rangle, \quad (5)$$

where

$$a1 = \frac{e^{\frac{1}{4}iJ\gamma t} [q^2 \cos(\frac{1}{4}Jqt) - i(\gamma - 2\sqrt{2})q \sin(\frac{1}{4}Jqt)]}{2q^2}, \quad (6)$$

$$b1 = -\frac{e^{\frac{1}{4}iJ\gamma t} [\sqrt{2}q^2 \cos(\frac{1}{4}Jqt) + i(4 + \sqrt{2}\gamma)q \sin(\frac{1}{4}Jqt)]}{2q^2}. \quad (7)$$

Thus that the pure-state density matrix of the three-site system at time t is defined by

$$\rho_1(t) = |\varphi_1(t)\rangle\langle\varphi_1(t)|. \quad (8)$$

In the product space of σ^z , $\rho_1(t)$ can be written as

$$\rho_1(t) = \begin{bmatrix} 0 & 0 & 0 & 0 & 0 & 0 & 0 & 0 \\ 0 & w & x & 0 & w & 0 & 0 & 0 \\ 0 & x^* & y & 0 & x^* & 0 & 0 & 0 \\ 0 & 0 & 0 & 0 & 0 & 0 & 0 & 0 \\ 0 & w & x & 0 & w & 0 & 0 & 0 \\ 0 & 0 & 0 & 0 & 0 & 0 & 0 & 0 \\ 0 & 0 & 0 & 0 & 0 & 0 & 0 & 0 \\ 0 & 0 & 0 & 0 & 0 & 0 & 0 & 0 \end{bmatrix}, \quad (9)$$

the expectation values of Pauli matrices and its correlation functions can be represented by the time-dependent density matrix,

$$\langle \sigma_1^z \rangle = y = \frac{1}{2} + \frac{2\sqrt{2}\gamma \sin^2(\frac{1}{4}Jqt)}{q^2}, \quad (10)$$

$$\langle \sigma_1^z \sigma_3^z \rangle = y - 2w = -\frac{4\sqrt{2}\gamma \sin^2(\frac{1}{4}Jqt)}{q^2}, \quad (11)$$

$$\langle \sigma_1^x \sigma_2^x \rangle = x + x^* = -\frac{8 + \gamma^2 \cos(\frac{1}{2}Jqt)}{\sqrt{2}q^2}, \quad (12)$$

$$\langle \sigma_1^x \sigma_2^y \rangle = ix - ix^* = -\frac{\gamma \sin(\frac{1}{2}Jqt)}{\sqrt{2}q}. \quad (13)$$

When γ is a fixed value, it can be seen that the mean value of σ_1^z and its correlation function are all periodic functions with respect to time based on Eqs. (10) to (13). Similarly, when q is a fixed value, each matrix element of $\rho_1(t)$ is also periodic function with respect to time because that each matrix element can be regarded as a function of the expectation value of Pauli matrix and its correlation function, as follows

$$w = \frac{1}{2}(\langle \sigma_1^z \rangle - \langle \sigma_1^z \sigma_3^z \rangle) = \frac{1}{4} - \frac{\sqrt{2}\gamma \sin^2(\frac{1}{4}Jqt)}{q^2}, \quad (14)$$

$$x = \frac{1}{2}(\langle \sigma_1^x \sigma_2^x \rangle - i \langle \sigma_1^x \sigma_2^y \rangle) = -\frac{8 + \gamma^2 \cos(\frac{1}{2}Jqt) - i\gamma q \sin(\frac{1}{2}Jqt)}{2\sqrt{2}q^2}, \quad (15)$$

$$y = -\langle \sigma_1^z \rangle = \frac{1}{2} + \frac{2\sqrt{2}\gamma \sin^2(\frac{1}{4}Jqt)}{q^2}. \quad (16)$$

It is well known that there are many measurement methods for pairwise entanglement [30–33]. In this paper, we calculate the concurrence of the system and observe the evolution rules of concurrence with time. In order to without loss of generality, we trace over site 2. The reduced density matrix for sites 1 and 3 can be obtained as

$$\rho_{13}(t) = \begin{bmatrix} y & 0 & 0 & 0 \\ 0 & w & w & 0 \\ 0 & w & w & 0 \\ 0 & 0 & 0 & 0 \end{bmatrix}. \quad (17)$$

The concurrence between the sites 1 and 3 is defined as

$$C_1(t) = \max\{\sqrt{\lambda_4} - \sqrt{\lambda_3} - \sqrt{\lambda_2} - \sqrt{\lambda_1}, 0\}, \quad (18)$$

where the $\lambda_k (k = 1, 2, 3, 4)$ are the eigenvalues of $\hat{R} = \rho_{13}(t)\tilde{\rho}_{13}(t)$ [with $\tilde{\rho}_{13}(t) = (\sigma_1^y \otimes \sigma_3^y)\rho_{13}^*(\sigma_1^y \otimes \sigma_3^y)$ is the spin-flipped density matrix operator] in ascending order. The eigenvalues of \hat{R} can be accurately solved:

$$\lambda_1 = \lambda_2 = \lambda_3 = 0, \quad \lambda_4 = 4w^2. \quad (19)$$

Therefore, the concurrence of the three-site system corresponding to the first quench procedure is obtained

$$C_1(t) = 2w = \langle \sigma_1^z \rangle - \langle \sigma_1^z \sigma_3^z \rangle = \frac{1}{2} - \frac{2\sqrt{2}\gamma \sin^2(\frac{1}{4}Jqt)}{q^2}. \quad (20)$$

When γ is a fixed value, the $C_1(t)$ is a periodic function with respect to time based on Eq. (20). The concurrence between spin blocks whose with different number of sites can be obtained by step by step iteratively QRG equation.

3.2. Spin z axis rotation quench

The three-site spin system is initialized on the ground state of Hamiltonian H_{02} ($H_{02} = -\frac{J}{4}[\sigma_1^x \sigma_2^x + \sigma_2^x \sigma_3^x + \sigma_1^y \sigma_2^y + \sigma_2^y \sigma_3^y - \gamma(\sigma_1^z \sigma_2^z + \sigma_2^z \sigma_3^z)]$) that it is obtained by rotating a π around the z axis for all even sites and leave all odd sites unchanged in the XXZ model, which can be achieved by pulsed laser in experimentally [25]. The initial state $|\varphi_{02}\rangle (|\varphi_{02}\rangle = \frac{d}{2} |\uparrow\uparrow\downarrow\rangle - \frac{q+\gamma}{2} |\uparrow\downarrow\uparrow\rangle + \frac{d}{2} |\downarrow\uparrow\uparrow\rangle)$ evolves under the Hamiltonian H of XXZ system when time $t = 0$, where $d = \sqrt{8 + (q + \gamma)^2}$. The state of the system evolves to $|\varphi_2(t)\rangle = e^{-iHt} |\varphi_{02}\rangle$. Thus that the time-dependent density matrix of three-site system can be written as

$$\rho_2(t) = |\varphi_2(t)\rangle \langle \varphi_2(t)|. \quad (21)$$

As we have mentioned above, each matrix element of $\rho_2(t)$ can also be derived from the average value of the Pauli matrix and its correlation functions, which is also periodic function with respect to time. We obtain the concurrence of sites 1 and 3 using the previous method. The concurrence is

$$C_2(t) = \frac{8\gamma - \gamma^3 + q^3 - 16\gamma \cos(\frac{1}{2}Jqt)}{2q^3}. \quad (22)$$

Obviously, $C_2(t)$ is a periodic function with respect to time when γ is a fixed value. Similarly, entanglement between larger spin blocks can be obtained by QRG equation. For simplicity and without loss of generality, we will choose the exchange coupling $J = 1.0$ afterwards.

3.3. Evolution of concurrence

It is easy to see from Eq. (20) and (22) that the concurrence of the system mainly depend on the time(t) and the anisotropy parameter(γ). For different QRG steps, $C_1(t)$ and $C_2(t)$ versus time(t) for the different values of γ is plotted in Fig. 1. As can be seen from Figs. 1(a1) and (a2), the $C_1(t)$ shows a cosine variations with time while $C_2(t)$ shows a sine change with time, but $C_1(t)$ and $C_2(t)$ have the same period($T = \frac{4\pi}{J\sqrt{8+\gamma^2}}$) with time. As shown in Fig. 1(a1) and (a2), as the size of the system increases, the lowest peak of $C_1(t)$ gradually becomes higher when $\gamma = 0.9$, conversely, each peak of $C_2(t)$ gradually decreases. It is interesting that the periods of $C_1(t)$ and $C_2(t)$ progressively become larger under QRG iteration and finally $C_1(t)$ and $C_2(t)$ are equal to 0.5 in the thermodynamic limit. As we have mentioned previously, the coupling constant flows to the stable fixed point($\gamma = 0$) under QRG iteration when $\gamma = 0.9$. At $\gamma = 0$, the initial Hamiltonian(H_{01}) and the evolutionary Hamiltonian(H) are the same so that the $C_1(t)$ does not change with time. For $\gamma = 1$ (see the left insets of Fig. 1(a1) and (a2)), the invariance between the concurrence of different-length chains is the result of the correlation length divergence at $\gamma_c = 1$. For $\gamma = 1.1$ (see in Fig. 1(a1) right inset), when the QRG iteration tends to infinity, the lowest peak of $C_1(t)$ decreases at first and then increases and finally oscillates around 0.5. In Fig. 1(a2) right inset, as the size of the system increases, the height of each peak of $C_2(t)$ increases at first and then decreases gradually and finally vanishes when $N \rightarrow \infty$. It is easy to see that increasing the length of the chain shortens the periods of $C_1(t)$ and $C_2(t)$ when $\gamma = 1.1$.

In order to further understand the evolution of entanglement, we calculate that the

probability of the evolved ground state returns to the initial ground state for two different quench types, separately [27, 28]. As follows

$$P_1 = |\langle \varphi_{01} | \varphi_1(t) \rangle|^2 = \frac{16 + \gamma^2 + \gamma^2 \cos(\frac{1}{2}qt)}{16 + 2\gamma^2}, \quad (23)$$

$$P_2 = |\langle \varphi_{02} | \varphi_2(t) \rangle|^2 = \frac{64 + \gamma^4 + 16\gamma^2 \cos(\frac{1}{2}qt)}{q^4}. \quad (24)$$

Higher values of P_1 and P_2 mean that the system is easier to return to the initial state, in addition, the system completely returns its initial state when $P_1 = 1$ or $P_2 = 1$. As can be seen from Eq. (23) and (24), for a fixed value of γ , P_1 and P_2 are periodic functions with respect to time and the periods are $T = \frac{4\pi}{\sqrt{8+\gamma^2}}$. It means that the system will completely return to the initial state every other period. In particular, the greater the γ , the shorter the period.

For different QRG steps, the evolution of $C_1(t)$ and $C_2(t)$ versus γ for $t = 11.5$ and $t = 1.5$ is plotted in Fig. 2. We find that the changes of concurrence corresponding to the two quenching methods with respect to anisotropy parameters are different, it means that initial state plays an important role in the evolution of system entanglement. Moreover, the short-time (sufficiently near to the initial moment) behavior and long-time (far from the initial moment) behavior of concurrence are somewhat different. As shown in Fig. 2(b1), at $t = 11.5$, the concurrence decreases from the equilibrium state to a finite value and then start to oscillate when the γ is turned on. However, at $t = 1.5$ (see in Fig. 2(b1) inset), the concurrence decays from equilibrium state to zero and then begin to oscillate. As γ increases, the values of each trough of $C_1(t)$ gradually high and finally severe oscillates around 0.5 when γ tend to infinity. It is because that the period of the system returns completely to the initial state approaches zero when γ tends to infinity, which can be obtained from Eq. (23), hence, $C_1(t)$ violently oscillates around 0.5 when $\gamma \rightarrow \infty$ because that the ground state entanglement of the initial Hamiltonian(H_{01}) equals 0.5 and it is independent of γ . The changes of $C_2(t)$ versus γ is different from $C_1(t)$ when $t = 11.5$ and $t = 1.5$. From the Fig. 2(b2), as γ increases, we find that the $C_2(t)$ increases from the initial state to a finite value and then begins to oscillate, but for $t = 1.5$ [see the inset of Figs. 2(b2)], the $C_2(t)$ reaches its maximum at first and then begins to oscillate. the height of each peak of $C_2(t)$ gradually decreases with γ increases and finally vanishes as $\gamma \rightarrow \infty$, it is because that the ground state entanglement of H_{02} is related to γ , i.e., the ground state entanglement of H_{02}

tends to zero when $\gamma \rightarrow \infty$. Although the change $C_1(t)$ and $C_2(t)$ versus γ are different, but they all reveal that increasing the length of the chain enhances the oscillation of the $C_1(t)$ and $C_2(t)$. Moreover, in the thermodynamic limit, $C_1(t)$ and $C_2(t)$ all happen mutation at the critical point because that the result of the correlation length divergence at $\gamma_c = 1$.

The non-analytic behavior of a physical quantity is a characteristic of QPT. The non-analytic behavior is often accompanied by a scaling behavior since that the correlation length diverges at the critical point. In this section, we demonstrate that the characteristic time can be used to describe the critical phenomenon of the one-dimensional anisotropic XXZ model which in the vicinity of the transition point. For any the anisotropy parameter, we define the characteristic time $T_{\min}^k(\gamma)$ at which the $C_1(t)$ reaches its k th minimum values and $T_{\max}^k(\gamma)$ at which the $C_2(t)$ reaches its k th maximum values. The characteristic time is analyzed as a function of the coupling constant(γ) at different QRG steps.

Further insight, we analyze the first derivatives of T_{\min} and T_{\max} with respect to the coupling constant(γ) for $k = 1$ in Fig. 3, which show the singular behavior at the critical point as the size of the system becomes large. The inset of Fig. 3 are the change of T_{\min} and T_{\max} versus γ at different QRG steps, which shows that T_{\min} and T_{\max} develop two saturated values in the thermodynamic limit. Specially, as shown in Fig. 3(c1) and Fig. 3(c2), $\frac{dT_{\min}}{d\gamma}$ and $\frac{dT_{\max}}{d\gamma}$ vs the γ are both of the same singular behavior because that the period of $C_1(t)$ and $C_2(t)$ are identical when the γ is a constant. For a more detailed analysis, the position of the minimum (γ_m) of $\frac{dT_{\min}}{d\gamma}$ approaches the critical point with the size of the system increase. This is plotted in Fig. 4, which shows the relation $\gamma_m = \gamma_c + N^{-\theta}$ with $\theta = 0.47$. Besides, the scaling behavior of $y \equiv \left| \frac{dT_{\min}}{d\gamma} \right|_{\gamma_m}$ versus N is plotted in Fig. 5 which shows a liner behavior of $\ln(y)$ versus $\ln(N)$, i.e., $\left| \frac{dT_{\min}}{d\gamma} \right|_{\gamma_m} \sim N^{0.46}$. Moreover, the exponent θ is directly related to the correlation length exponent ν at the vicinity of critical point (γ_c), i.e., the relation is $\theta = \frac{1}{\nu}$. Interestingly, the characteristic time represents scaling behavior close to the quantum critical point with exponent $\theta = 0.47$ which fantastic corresponds to the entanglement exponent of the one-dimensional XXZ model. Remarkably, the scaling behavior of $\left| \frac{dT_{\max}}{d\gamma} \right|_{\gamma_m}$ versus N is the same as $\left| \frac{dT_{\min}}{d\gamma} \right|_{\gamma_m}$ because that $C_1(t)$ and $C_2(t)$ have the same period when γ is a constant. Therefore, we only study one of them.

4. SUMMARY

In this paper, the dynamics of entanglement for the one-dimensional spin- $\frac{1}{2}$ anisotropic XXZ model are studied using the quantum renormalization-group method. We obtain the analytic expressions of concurrence of the system corresponding to two different quenching methods. We find that the initial state plays a key role in the evolution of system entanglement. In order to further understand the dynamics of system entanglement, we investigate the probabilities when the system return to the initial state Corresponding to the two quenching methods, the result shows that both of them return completely to the initial state with period($T = \frac{4\pi}{\sqrt{8+\gamma^2}}$). The period is related to the anisotropy parameter, i.e., when $\gamma \rightarrow \infty$, the period when the system returns completely to the initial state approaches zero. We demonstrate that the characteristic time can detect the QPT of one-dimensional XXZ model. Interestingly, we find that the scaling behavior of $\left| \frac{dT_{\max}}{d\gamma} \right|_{\gamma_m}$ versus N close to the critical point are similar to those of the XXZ model in equilibrium and find the scaling behavior is independent of the initial state or quenching method.

Acknowledgments

This work was supported by the National Natural Science foundation of China under Grant NO. 11847086, NO. 11675090.

-
- [1] J. S. Bell, Physics (Long Island City, NY) **1**, 195 (1964).
 - [2] M. A. Nielsen and I. L. Chuang, Quantum Computation and Quantum Communication (Cambridge University Press, Cambridge, 2000).
 - [3] A. Osterloh, L. Amico, G. Falci and R. Fazio, Nature (London) **416**, 608 (2002).
 - [4] S. Sachdev, Quantum Phase Transitions (Cambridge University Press, Cambridge, 2000).
 - [5] T. J. Osborne and M. A. Nielsen, Phys. Rev. A **66**, 032110 (2002).
 - [6] M. Kargarian, R. Jafari and A. Langari, Phys. Rev. A **76**, 060304 (2007).
 - [7] M. Kargarian, R. Jafari and A. Langari, Phys. Rev. A **77**, 032346 (2008).
 - [8] F.-W. Ma, S.-X. Liu and X.-M. Kong, Phys. Rev. A **83**, 062309 (2011); **84**, 042302 (2011).

- [9] Y.-L. Xu, X.-M. Kong, Z.-Q. Liu and C.-Y. Wang, *Phys. A (Amsterdam, Neth.)* **446**, 217 (2016).
- [10] Y.-L. Xu, L.-S. Wang and X.-M. Kong, *Phys. Rev. A* **87**, 012312 (2013).
- [11] M. Kargarian, R. Jafari and A. Langari, *Phys. Rev. A* **79**, 042319 (2009).
- [12] Y.-L. Xu, X. Zhang, Z.-Q. Liu, X.-M. Kong and T.-q. Ren, *Eur. Phys. J. B* **87**, 132 (2014).
- [13] Y.-L. Xu, X.-M. Kong, Z.-Q. Liu and C.-C Yin, *Phys. A* **95**, 042327 (2017).
- [14] A. Lamacraft and J. Moore, *Ultracold Bosonic and Fermionic Gases* (Elsevier, Oxford, UK, 2012), Vol. 5.
- [15] N. Gedik, D.-S. Yang, G. Logvenov, I. Bozovic and A. H. Zewail, *Science* **316**, 425 (2007).
- [16] Amico, L., A. Osterloh, F. Plastina, G. Palma and R. Fazio, *Phys. Rev. A* **69**, 022304 (2004).
- [17] S. D. Hamieh and M. I. Katsnelson, *Phys. Rev. A* **72**, 032316 (2005).
- [18] M. J. Hartmann, M. E. Reuter and M. B. Plenio, *New J. Phys.* **8**, 94 (2006).
- [19] Jie Ren and Shiqun Zhu, *Phys. Rev. A* **81**, 014302 (2010).
- [20] R. Jafari, *Phys. Rev. A* **82**, 052317 (2010).
- [21] P. Jurcevic, H. Shen, P. Hauke, C. Maier, T. Brydges, C. Hempel, B. P. Lanyon, M. Heyl, R. Blatt and C. F. Roos, *Phys. Rev. L* **119**, 080501 (2017).
- [22] R Jafari, *J. Phys. A* **49**, 185004 (2016).
- [23] J. Eisert, M. Friesdorf and C. Gogolin, *Nat. Phys.* **11**, 124 (2015).
- [24] M. A. Martin-Delgado and G. Sierra, *Int. J. Mod. Phys. A* **11**, 3145 (1996).
- [25] A. Langari, *Phys. Rev. B* **58**, 14467 (1998).
- [26] R. A. Kaden, Hazzard, V. D. W. Mauritz, F.-F. Michael, R. Salvatore, Manmana, G. Emanuele, T. Dalla, P. Tilman, K. Michael and M. R. Ana, *Phys. Rev. A* **90**, 063622 (2014).
- [27] F. Verstraete, J. I. Cirac, J. I. Latorre, E. Rico and M. M. Wolf, *Phys. Rev. Lett.* **94**, 140601 (2005).
- [28] A. Rajak and U. Divakaran, *J. Stat. Mech.* P04023 (2014).
- [29] A. Dutta, G. Aeppli, B. K. Chakrabarti, U. Divakaran, T. Rosenbaum and D. Sen, *Quantum Phase Transitions in Transverse Field Spin Models: From Statistical Physics to Quantum Information* (Cambridge: Cambridge University Press, 2015).
- [30] Y. X. Chen and D. Yang, *Quant. Info. Proc.* **1**, 389 (2003).
- [31] G. Vidal and R. F. Werner, *Phys. Rev. A* **65**, 032314 (2002).
- [32] E. M. Rains, *Phys. Rev. A* **60**, 179 (1999).

[33] S. Hill and W. K. Wootters, Phys. Rev. Lett. **78**, 5022 (1997); W. K. Wootters, *ibid.* **80**, 2245 (1998).

Figure Captions

Fig. 1 (Color online) For different QRG steps, $C_1(t)$ and $C_2(t)$ change with time t . Where, the left inset corresponds to $\gamma = 1$ and the right panel corresponds to $\gamma = 1.1$.

Fig. 2 (Color online) Evolution of the concurrence versus γ for different values of time in terms of QRG iterations. The inset shows the change of $C_1(t)$ and $C_2(t)$ with anisotropy parameters at $t = 1.5$ and Figs. 2. (b1) and (b2) correspond to the $t = 11.5$, which is relatively large compared with 1.5.

Fig. 3 (color online) First derivative of T_{\min} and T_{\max} and their manifestation toward diverging as the number of QRG iteration increase. Inset: Evolution of T_{\min} and T_{\max} with respect to the anisotropy parameter as the number of QRG iterations increase.

Fig. 4 The scaling behavior of γ_m for different-length chains, where, γ_m is the position of minimum of $\frac{dT_{\min}}{d\gamma}$ in Fig. 3(c1).

Fig. 5 The scaling behavior of $\left| \frac{dT_{\min}}{d\gamma} \right|_{\gamma_m}$ versus system size N .

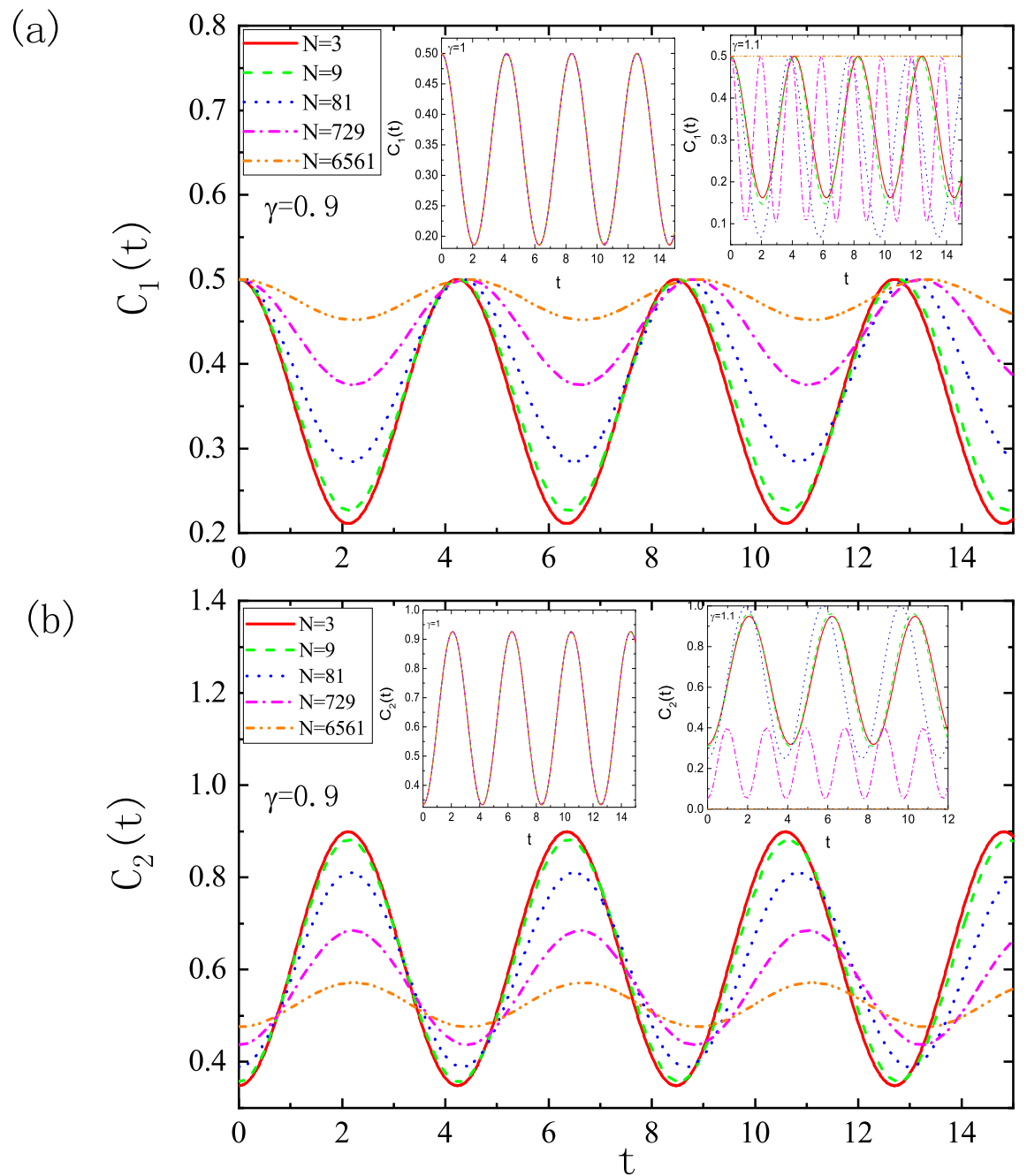


Figure 1

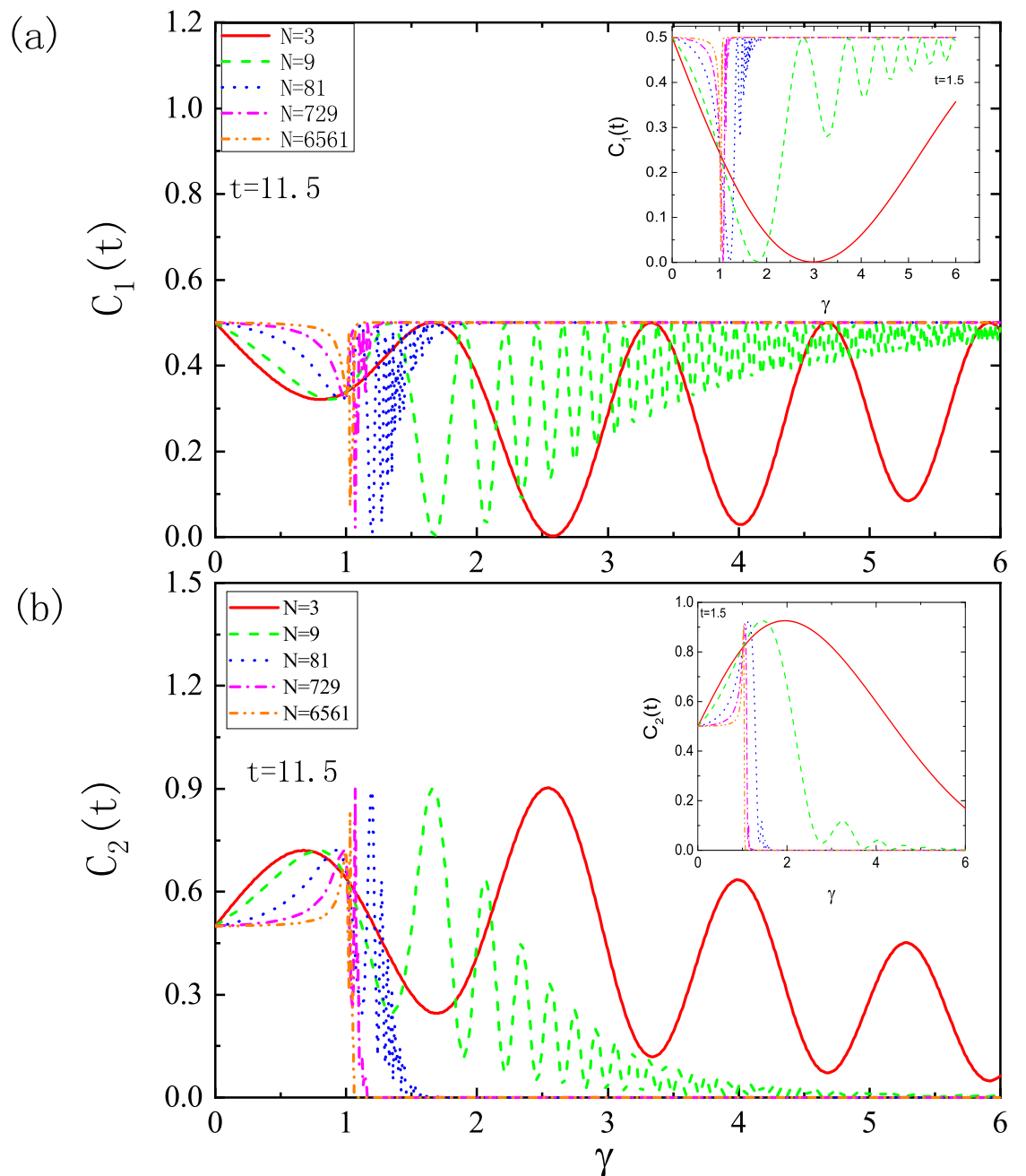
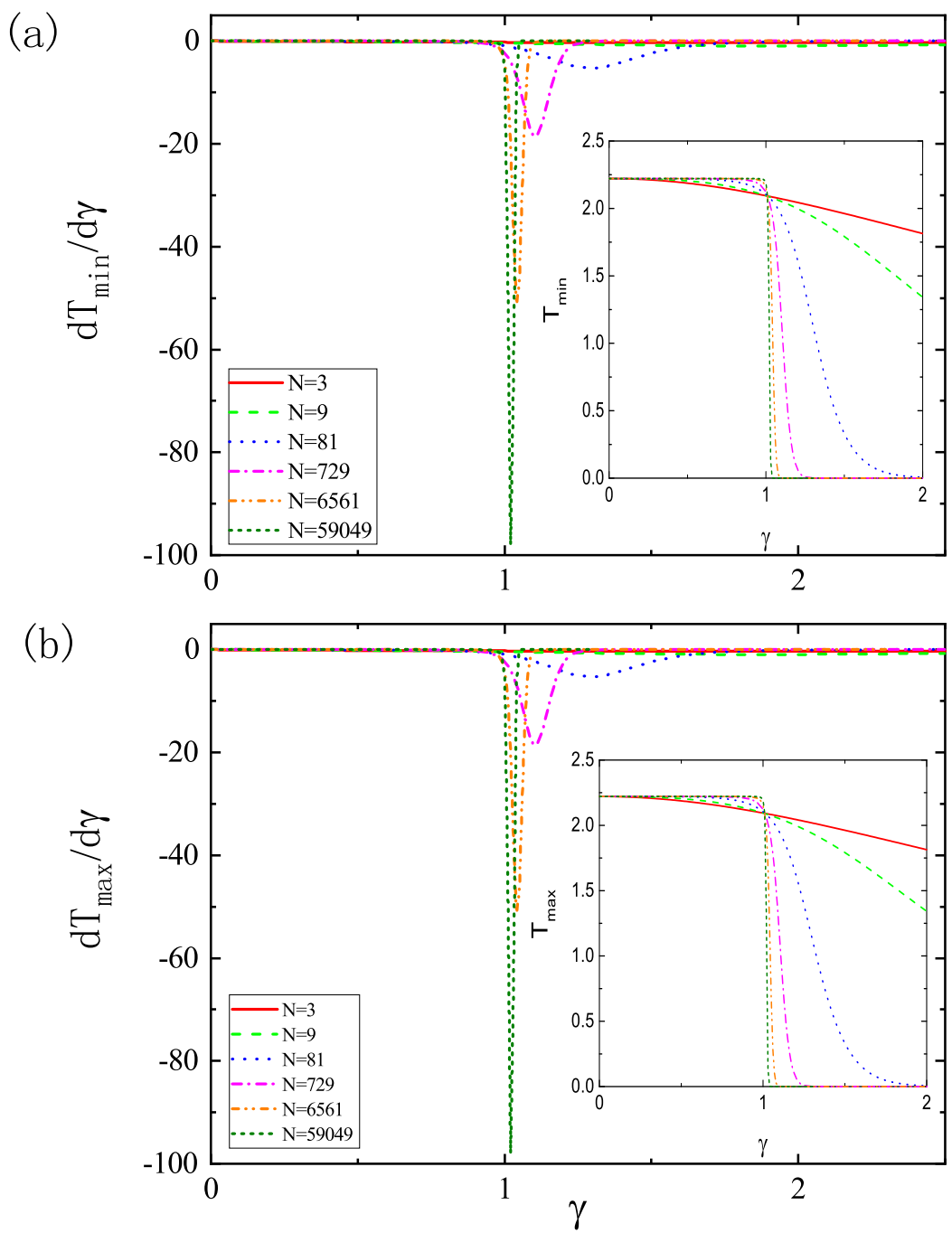


Figure 2



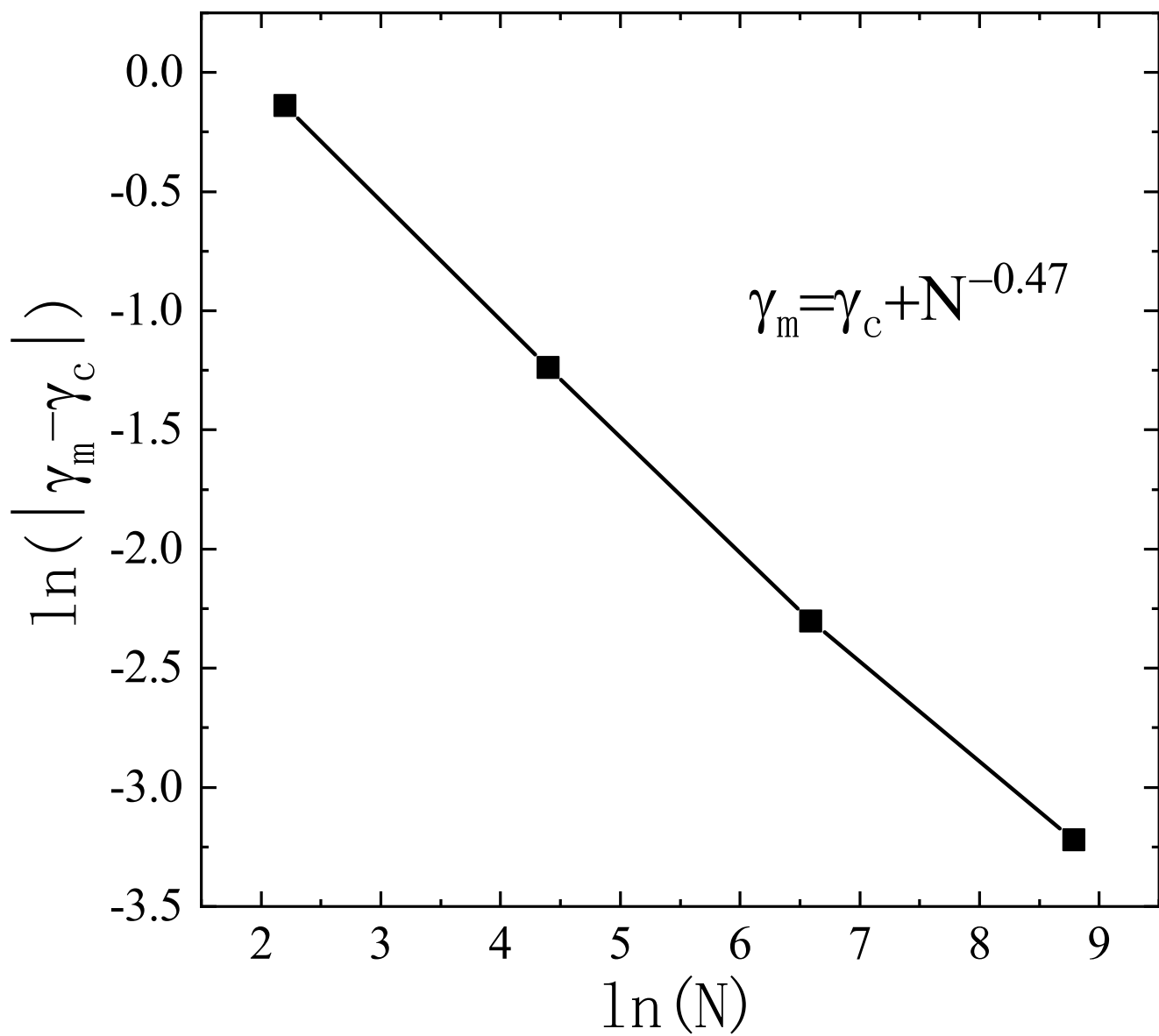


Figure 4

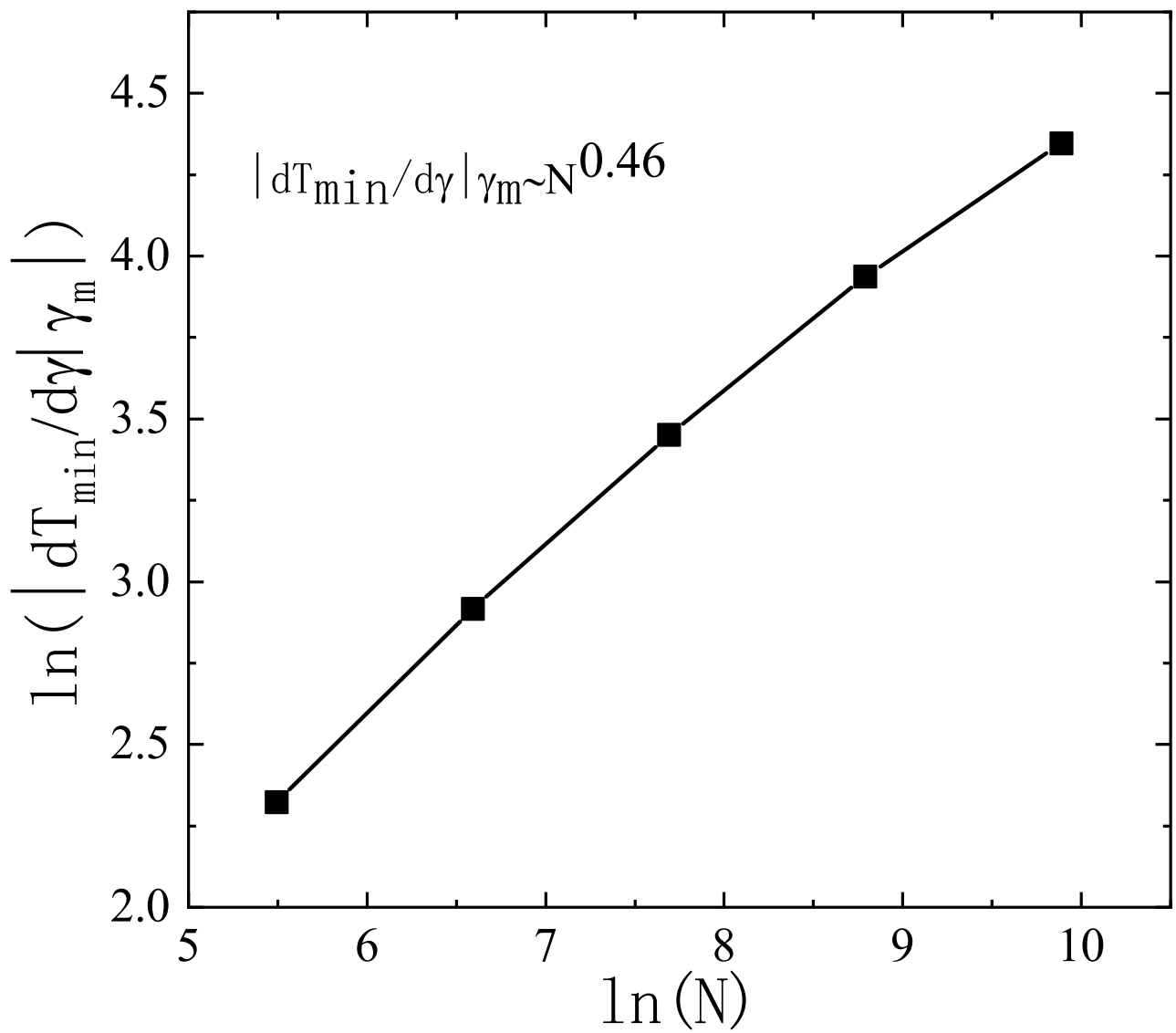


Figure 5